Unexpected Dual-Action of Cetyltrimethylammonium Bromide (CTAB) in the Self-Assembly of Colloidal Nanoparticles at Liquid-Liquid Interfaces

Queen's University Belfast - Research Portal:
Link to publication record in Queen's University Belfast Research Portal

Unexpected Dual Action of Cetyltrimethylammonium Bromide (CTAB) in the Self-Assembly of Colloidal Nanoparticles at Liquid–Liquid Interfaces

Chunchun Li, Yikai Xu,* Xinyuan Li, Ziwei Ye, Chaoyi Yao, Qinglu Chen, Yuanfeng Zhang, and Steven E. J. Bell*

Self-assembly of colloidal nanoparticles at water–oil interfaces offers an efficient way to construct multi-dimensional arrays. Self-assembly is generally induced by using adsorbing molecular "modifiers" or co-solvents to remove the nanoparticles' surface charge. Here, it is shown that cetyltrimethylammonium bromide (CTAB), which is commonly used in bulk quantities in colloidal synthesis, can induce self-assembly of negatively charged colloidal nanoparticles at water–oil interfaces, even at sub-micromolar levels but it does this by providing charge screening rather than removing the surface charge. Since this is a physical effect, CTAB can promote assembly of nanoparticles regardless of their morphology or material composition. In the specific case of nanoparticles which allow CTAB to adsorb, such as Au, the self-assembly mechanism switches from charge screening to chemical adsorption as the concentration is increased. These both explain previous observations of spontaneous interfacial assembly and open up further possibilities for deliberately constructing functional nanoparticle arrays without the need for additional modifiers or co-solvents.

1. Introduction

Nanoparticles (NPs) often exhibit properties which differ enormously from their bulk counterparts due to their exceptionally large surface areas and unique quantum structures.[1] These properties have led to applications of NPs in a wide variety of fields ranging from catalysis to sensing.[2,3] To achieve even more advanced functionalities, NPs can be used as functional building blocks to construct multi-dimensional arrays.[4] An

elegant and effective way to obtain 2D NP arrays is through bottom-up self-assembly of colloidal particles at the interface between two immiscible liquids.[5–8]

We are interested in preparing interfacial NP arrays using methods which cause minimum perturbation of the NP surface chemistry so that the chemical properties of the constituent particles are retained in the array. In particular, it is important to avoid modifying the surfaces of particles through adsorption of strongly bound molecular passivating layers because these will interfere with the functionality of the array, e.g., by preventing intimate contact between the surface and reactants in catalysis or hindering the close approach of target analytes to the surface which is essential for surface-enhanced Raman spectroscopy (SERS).[9,10]

The ideal method for interfacial assembly would be one in which the initial colloidal suspension is simply shaken with pure nonaqueous solvent and the particles spontaneously migrate to the interface. Unfortunately, while adsorption of solid NPs to liquid–liquid interfaces (LLIs) is highly favorable, since it significantly lowers the energy of the interface, this is counterbalanced by electrostatic repulsion between NPs. This means that NPs seldom spontaneously migrate to LLIs in significant numbers when aqueous colloids are simply mixed with highly immiscible oils.[11] Conventionally, films may be formed by functionalizing the surfaces of charged colloidal NPs with charge-neutral organic "modifiers" to reduce repulsion but this means that the surface of the NPs is covered in a layer of strongly adsorbed organic capping agents, which is undesirable for the reasons outlined above.[12,13] Alternatively, less polar co-solvents such as acetone and ethanol may be added, which reduce the ability of the aqueous phase to solvate ionic compounds and again significantly weaken the electrostatic repulsion between NPs.[14,15] Although this method can be readily applied to assemble various types of NPs, the loss of surface charge also leads to unwanted aggregation of the particles and the formation of structural defects in the product NP array.[16]

We have previously shown a third approach to induce self-assembly of colloidal NPs into defect-free NP arrays, which is based on adding amphiphilic salts to the biphasic system.[10,17,18]

C. Li, Dr. Y. Xu, X. Li, Dr. Z. Ye, Dr. C. Yao, Q. Chen, Y. Zhang, Prof. S. E. J. Bell
School of Chemistry and Chemical Engineering
Queen's University Belfast
University Road, Belfast BT9 5AG, UK
E-mail: yxu18@qub.ac.uk; S.Bell@qub.ac.uk

If the salts contain ions which are of opposite charge to the NPs and are also soluble in the organic layer, they can screen the charge repulsion between the particles in both the aqueous and organic layers and thus allow NPs to assemble in close proximity to each other at the interface. Examples of these promoters include tetrabutylammonium (TBA$^+$) salts, which are effective for assembling NPs with negative ζ potentials and tetrafluoroborate (TPB$^-$) salts for positively charged NPs. This "promoter" approach provides minimal perturbation of the system since the promoters do not chemically adsorb onto the particles and are present in low (typically µM) concentrations but it does require addition of an external agent.

In contrast to the established methods described above, recent reports have shown that citrate-capped gold nanorods can assemble at LLIs without the need for any additional components, other than the nonaqueous solvent layer, despite being highly charged.[19–22] This implies that there is a novel mechanism for interfacial assembly that allows the "ideal" case to be achieved experimentally. However, the underlying mechanism of this process has yet to be established.

Here, we explore this phenomenon in detail and present evidence that even trace amounts of cetyltrimethylammonium bromide (CTAB) surfactant, which is often present in colloids, especially Au nanorods, can induce NP self-assembly at LLIs. Interestingly, our experiments also revealed that CTAB's role in inducing interfacial self-assembly of citrate-stabilized Au NPs switches between promoter and modifier depending on its concentration, which is different from previously reported mechanisms of CTAB-induced self-assembly of polystyrene/silica NPs or any other previously reported promoter/modifier compounds.[23–25] This understanding is significant since it rationalizes existing data and opens up the possibility of generally assembling colloidal NPs at LLIs using either residual or deliberately added CTAB. We have illustrated this possibility by forming NP arrays at LLIs with a variety of extremely different negatively charged colloidal NPs, including, Au, Pt, SiO$_2$, TiO$_2$, and Au+SiO$_2$ composites, using CTAB. CTAB is the best-known representative of a large class of charged surfactants which are widely used as site-governing agents in synthesis of colloidal particles.[26,27] The discovery here that CTAB can induce interfacial self-assembly even at sub-µM concentrations bridges a critical gap between the synthesis of colloidal NPs and their further construction into functional multi-dimensional arrays.

2. Results and Discussion

One clear difference between the Au nanorods which show apparent promoter-free assembly and other NPs we have investigated previously is that the nanorods were synthesized in the presence of very high concentrations (≈0.1 M) of CTAB, which acted as a shape directing ligand and stabilizing agent.[28] However, these high surfactant concentrations are undesirable, e.g., very significant emulsification is observed if immiscible solvents are added. Therefore, in experiments aimed at interfacial assembly, the Au nanorods were treated using a two-step process, after which the colloid was said to contain only "trace amounts" of CTAB while the surface of the Au nanorods was capped with negatively charged citrate molecules.[29] With this

method, the exact amount of residual CTAB is difficult to establish and so in our work we took the approach of adding known concentrations of stock CTAB solution into citrate-reduced Au NPs synthesized without CTAB, which allowed us to precisely control the concentration of CTAB in our studies.

As illustrated in **Figure 1**a–c, in a typical experiment, citrate-reduced gold colloid (CRGC) was mixed with the required amount of CTAB and the immiscible oil (dichloromethane, DCM) before being shaken vigorously. As shown in Figure 1d, a lustrous metal-liquid like film (MeLLF) was formed at the LLI CTAB concentrations between 5×10^{-6} and 8×10^{-5} M. For the convenience of illustration, all CTAB concentrations refer to the concentration of the CTAB feedstock (as shown in Supporting Information S1, the final concentration of CTAB is ≈0.07 times the feedstock concentration). Above this concentration range significant emulsification occurred while below this range no apparent changes were observed. Figure 1e shows scanning electron microscope (SEM) images of a typical Au MeLLF which was prepared using 10^{-5} M CTAB feedstock and where the particles were subsequently fixed in position by forming in situ a polystyrene backing layer which allowed them to be removed from the LLI for imaging while preserving their initial packing order at the interface.[30] The image shows a densely packed and defect-free monolayer of NPs. As shown in Figure 1f, the extinction spectra of the Au MeLLFs (ii) and the parent colloid (i) show that in the Au MeLLFs there is strong extinction over a broad wavelength range, which is due to strong electron coupling between the densely packed NPs at the interface.

The experiments above showed that an appropriate amount of CTAB in solution is clearly critical for inducing NP self-assembly. To further investigate the role of CTAB in NP-self-assembly process, in situ SERS measurements of the Au MeLLFs were performed to study the surface chemistry of the Au NPs before and after self-assembly. Interestingly, the SERS signals from CRGC MeLLFs formed using CTAB changed dramatically with the concentration of CTAB. The spectra labeled as set (i) in **Figure 2**a show the typical SERS signals acquired from CRGC MeLLFs formed using lower CTAB feedstock concentrations (5–9×10^{-6} M). There was a weak Au-Br vibration (180 cm^{-1}), which arose from the small amount of adsorbed Br$^-$ species from CTAB and as a result, grew with the increasing concentration of CTAB. However, in general the SERS signals were dominated by vibrational bands which can be attributed to Au-Cl (250 cm^{-1}), citric acid, and various oxidants of citric acid (1537, 1432, 1374, 1300, 1246, 1165, 994, 760, and 492 cm^{-1}) initially present on the surface of the Au NPs.[31–33] These data suggest that in this concentration range the amount of CTAB adsorbed on the surface of the particles is small and thus it should have a negligible effect on their surface properties. Indeed, the ζ potential of CRGC is barely affected by the addition of CTAB at this feedstock concentration range and the NPs remain highly charged (≤−30 mV), as shown in Figure 2b-i. However, at CTAB feedstock concentrations above 9×10^{-6} M the intensity of the signals from the initial surface species significantly reduced and the spectra became increasingly dominated by CTAB bands at 1441, 1296, 760, and 180 cm^{-1}, which shows that large amounts of CTAB was adsorbing onto the NPs' surface.[34] This effect is also clearly shown by the corresponding ζ potentials of the NPs at these increasing CTAB

**ADVANCED
SCIENCE NEWS**
www.advancedsciencenews.com

**ADVANCED
MATERIALS
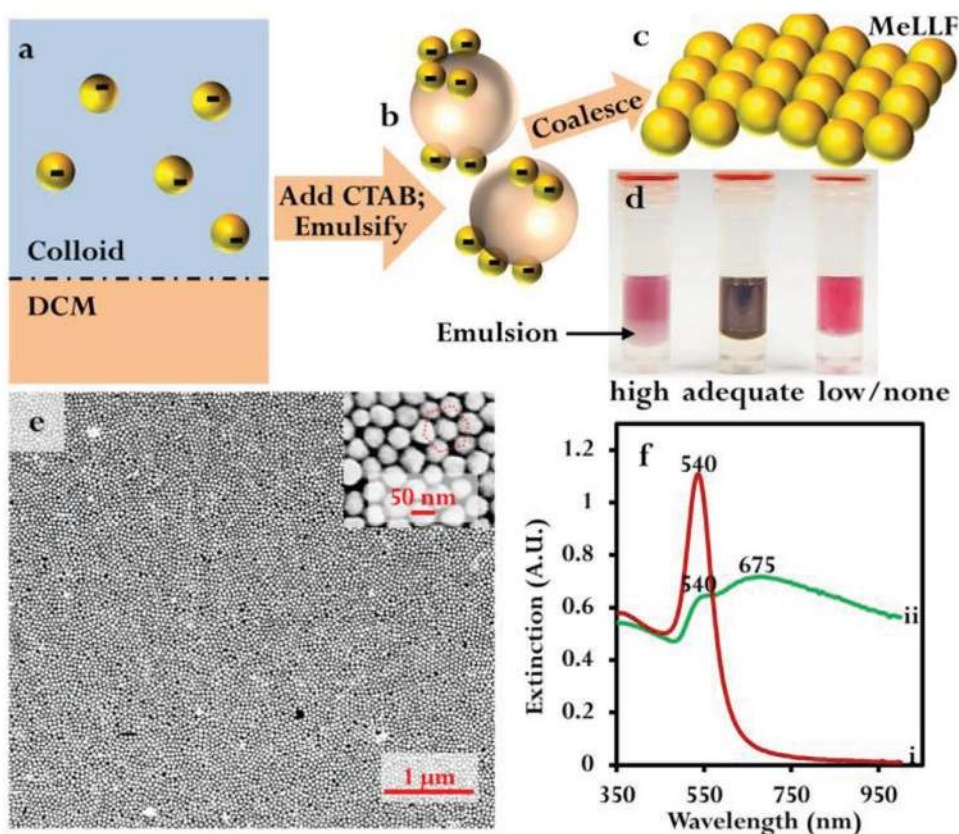INTERFACES**
www.advmatinterfaces.de

Figure 1. a–c) Schematic illustrations of CTAB-induced self-assembly of negatively charged citrate-reduced gold colloid (CRGC) NPs at a water–dichloromethane (DCM) interface. d) Optical image of CRGC and DCM mixed with CTAB at different concentrations, at the highest concentration the sample is emulsified. e) SEM images of CRGC metal-liquid like film (MeLLF) formed with 10^{-5} M CTAB feedstock. The high-magnification inset image shows the NPs packed in hexagonal order. f) UV/vis extinction spectra of i) CRGC colloid and ii) CRGC MeLLF formed with 10^{-5} M CTAB feedstock.

feedstock concentrations which gradually moved toward, and finally stabilized at, zero (see Figure 2b-ii,iii). To ensure that this effect was not simply due to the adsorption of just Br$^-$ ions from CTAB or large changes in the local ionic strength of the colloid, contrast ζ potential measurements were also performed on CRGC mixed with NaBr solutions at the same concentrations as CTAB. The results showed that within the relevant concentration range, addition of NaBr had the opposite effect on the colloids compared to CTAB and led to a more negative ζ potential, which demonstrated that the CTA$^+$ component must play a significant role in the ζ potential change of CRGC observed with the addition of CTAB (Figure S1, Supporting Information).

As discussed above, the key for inducing self-assembly of charged colloidal NPs into tightly packed interfacial arrays is to lower the interparticle aggregation barrier which arises from strong interparticle electrostatic repulsion as described by the classic DVLO (Derjaguin, Landau, Vervey, and Overbeek) theory.[35] This has been achieved either by removing the NPs' surface charge with modifiers or screening with promoters, however, the SERS and ζ potential data in Figure 2a,b suggest that CTAB induces CRGC self-assembly through two different mechanisms, acting as modifier and/or promoter depending on its concentration. As shown in **Figure 3**a, at the high-end of the appropriate CTAB concentration range CTAB behaves as a modifier and adsorbs directly onto the surface of the NPs to form

a monolayer of CTAB comprising chemisorbed Br$^-$ ion paired to CTA$^+$, which is evident by the SERS spectra of the product NP array becoming dominated by CTAB signals. Importantly, at this concentration region there is not enough free CTA$^+$ to form a charged bilayer on the NPs' surface like that in CTAB-stabilized positively charged Au nanorods.[36] Instead, it is the hydrophobic alkyl chain tails of CTAB which are directed outward, so the NPs are charge neutral, as shown in our ζ potential measurements.[23,37] Conversely, at the low end of the CTAB concentration range, SERS data show that the amount of CTAB directly adsorbed on the surface of the NPs is extremely low. As a result, the NPs remain highly charged with ζ lower than -30 mV. It is well established that amphiphilic molecules such as CTAB have the tendency to partition from water into nonpolar organic solvents, such as DCM.[38,39] Moreover, we have previously shown that various organo-ions, from tetrabutyl cations to crown ether-Na$^+$ complexes, can transfer from aqueous solution into organic solvents to act as promoters for NP-interfacial self-assembly.[17,18,40] For CTAB, the dissociation into CTA$^+$ and Br$^-$ in the organic phase is also likely to be aided by the small amount of dissolved water in the DCM. The result is that although at lower concentrations there is insufficient CTAB adsorbed on the surface of Au NPs to induce NP self-assembly by acting as a modifier, there is still sufficient free CTA$^+$ in the organic phase, to promote self-assembly through charge-screening
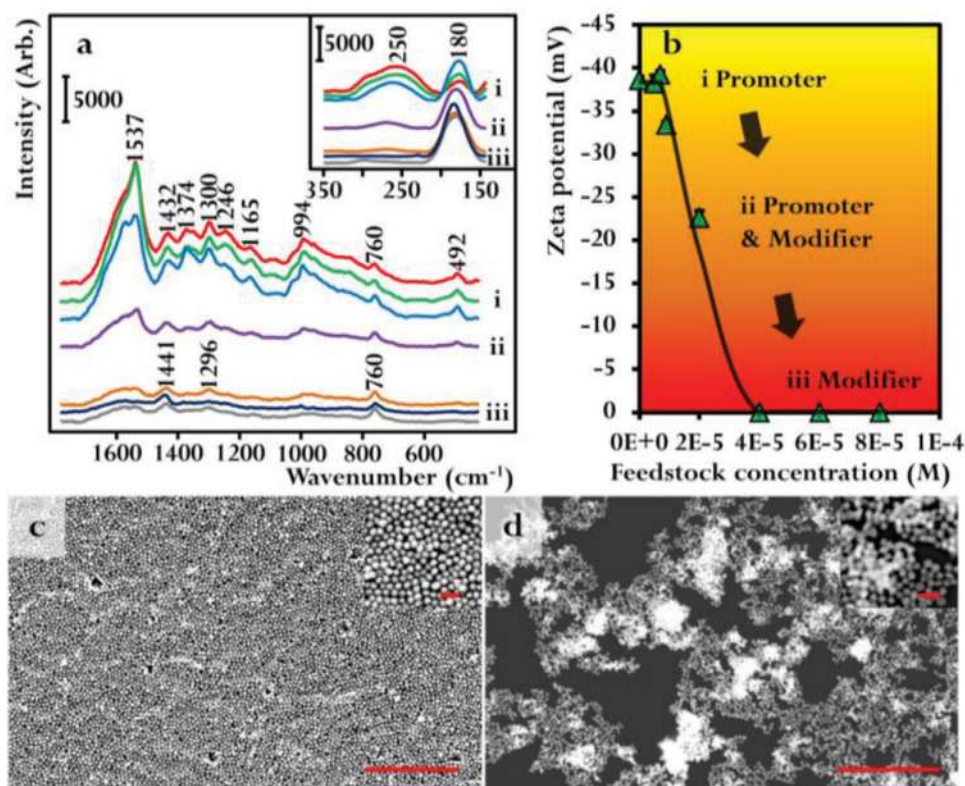
**ADVANCED
SCIENCE NEWS**

www.advancedsciencenews.com

**ADVANCED
MATERIALS
INTERFACES**

www.advmatinterfaces.de

Figure 2. a) From top to bottom are SERS spectra acquired from CRGC MeLLFs formed using i) 5×10^{-6}, 7×10^{-6}, 9×10^{-6}; ii) 2×10^{-5}; iii) 4×10^{-5}, 6×10^{-5}, and 8×10^{-5} M CTAB feedstock. b) Plot showing the average ζ potential of CRGC at i–iii) CTAB feedstock concentration ranges corresponding to the SERS data. c,d) SEM image of a typical CRGC MeLLF formed using CTAB as promoter (7×10^{-6} M) and modifier (6×10^{-5} M), respectively. Insets show high-magnification SEM image of the samples. Scale bars in low- and high-magnification images correspond to 1 μm and 50 nm, respectively.

on the oil side of the LLI, as shown in Figure 3b. This correlates well with previous reports where CTAB was found to be able to stabilize negatively charged polystyrene and silica NPs at liquid–air interfaces by providing electrostatic charge screening.[41] This effect, when combined with charge screening provided by hydrophilic cations inherently present in the aqueous phase and interparticle van der Waals attraction, allows NPs to self-assemble into tightly packed monolayers at the LLI. Of course, the amount of CTA+ required to achieve sufficient screening will vary depending on factors such as NP's surface charge and hydrophobicity. However, the amount of free CTA+ required to provide sufficient interparticle charge screening in the oil phase to induce NP self-assembly is much lower than the amount of CTAB modifier required for complete charge removal. This is partly because charged NPs are generally hydrophilic so only a small proportion of each particle will be submerged in the oil phase upon self-assembly. In addition, some of the charged hydrophilic species on the NPs' surface will either desorb or recombine with counter ions upon entering the oil phase.[42] Therefore, only a part of the initial surface charge will be retained on the parts of NPs immersed in the oil phase.

In the intermediate CTAB concentration range, there is enough CTAB directly adsorbed on the surface of the NPs to generate a notable decrease in interparticle electrostatic repulsion. However, this is not sufficient to allow the NPs to self-assemble at the LLI, and the free-CTA+ in solution is also required to screen the remaining negative charge between NPs at the interface.

Therefore, at this concentration range CTAB takes on the dual role of modifier and promoter, as illustrated in Figure 3c.

The differences in the NP self-assembly mechanism at different CTAB concentration also lead to notably different particle packing in the product MeLLFs. Figure 2c,d shows SEM images of typical Au MeLLFs formed under identical experimental conditions, apart from using CTAB concentrations where it acted as a promoter or modifier, respectively. Since the interparticle electrostatic repulsion was completely removed at high CTAB concentrations, the NPs had a much higher tendency to form aggregates at the interface so the resulting Au MeLLFs contained large amounts of defects and 3D aggregates. Conversely, Au MeLLFs formed using CTAB as promoter exhibited highly ordered hexagonal packing.

The result of these considerations is that the role of CTAB in the interfacial self-assembly of citrate-stabilized Au NPs is complex and depends strongly on the concentration of CTAB, switching from formation of an adsorbed charge-neutral layer at higher concentrations to being a nonabsorbing charge screening agent at lower concentrations within a narrow concentration range. It is worth noting that CTAB is the first compound found to combine the ability to act as both modifier and promoter in inducing interfacial NP self-assembly. The fact that CTAB can act as a promoter is significant since this means that it can still be used to promote Au MeLLF formation even when the surface of the NPs is functionalized with negatively charged capping agents with stronger affinity towards Au surfaces than
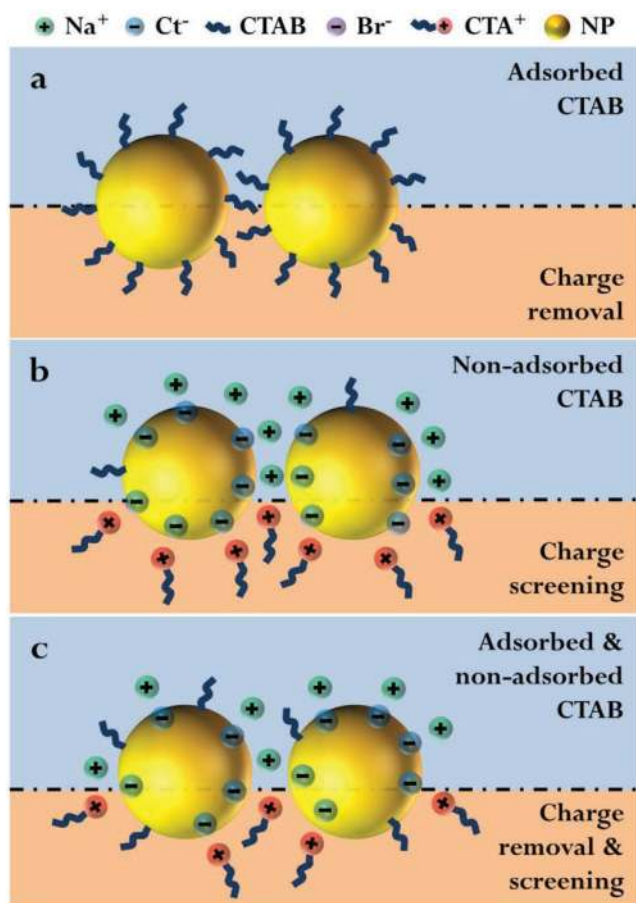
ADVANCED
SCIENCE NEWS
www.advancedsciencenews.com

ADVANCED
MATERIALS
INTERFACES
www.advmatinterfaces.de

Figure 3. Schematic illustration of the mechanism of CTAB inducing self-assembly of negatively charged colloidal Au NPs at LLIs through a) charge removal, b) charge screening, or c) a combination of charge removal and charge screening. For clarity, only ions near the particle surfaces are shown and dissociated CTA$^+$, Br$^-$, and undissociated CTAB in the bulk aqueous and oil layers have been omitted.

Figure 4. SERS signals obtained from a control sample of i) MPS-modified CRGC aggregated with 1 M (NH$_4$)$_2$SO$_4$ and ii) an MPS-modified CRGC MeLLF formed with 4×10^{-5} M CTAB feedstock. The spectra have been rescaled for illustration.

to promote the formation of densely packed NP arrays at LLIs using single or even multiple types of negatively charged colloidal NPs, regardless of their surface chemistry, particle morphologies, or material compositions. **Figure 5**a,b shows SEM images of negatively charged P25 TiO$_2$ NPs and SiO$_2$ NPs assembled into densely packed monolayer films using 10^{-5} M CTAB feedstock solution. As shown in the inset high-magnification SEM images, the TiO$_2$ NPs were packed randomly due

CTAB, such as thiols. To illustrate this possibility, the surface of CRGC was pre-functionalized with charged thiol modifiers to produce thiol-modified Au colloids with typical zeta potentials of −45 mV (Table S2, Supporting Information). More importantly, these surface-modified Au NPs could still be induced to assemble into MeLLFs using CTAB, and their SERS signatures remained unchanged and were dominated by the SERS signals of the thiol modifiers before and after self-assembly even at the high CTAB concentrations (**Figure 4**, see Figure S2 in the Supporting Information for another example). As shown in Figure 4-i,ii, electrostatic interaction between the CTA$^+$ promoter and SO$_3^-$ group in the 3-mercapto-1-propane sulfonate (MPS$^-$) surface ligands causes a red shift of the 1074 cm^{-1} peak to 1057 cm^{-1}.[43] Conversely, when Au colloids were pre-functionalized with positively charged thiols, such as thiocholine, NP self-assembly could not be induced using CTAB.

Since CTAB can induce NP self-assembly through electrostatic charge screening, which does not require CTAB to chemically adsorb onto the particle surface, this means that the ability of CTAB to promote NP interfacial self-assembly is not material specific. Therefore, CTAB can be generally used
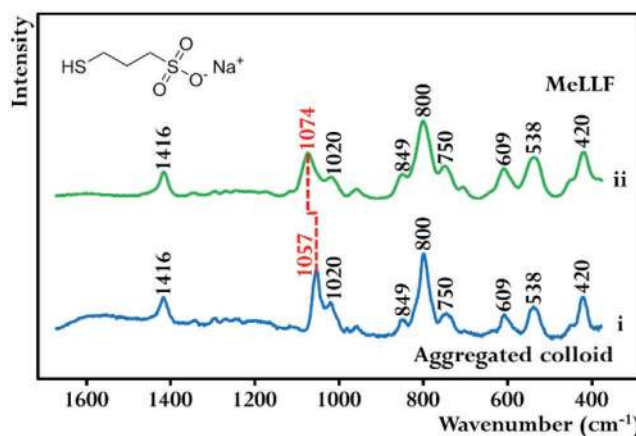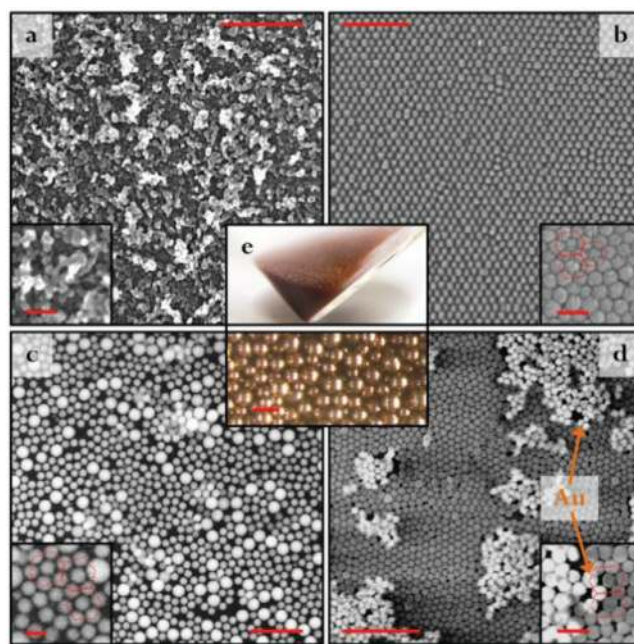

Figure 5. SEM images of CTAB-induced self-assembled 2D NP arrays formed using: a) poly-disperse TiO$_2$ NPs; b) spherical SiO$_2$ NPs; c) spherical Pt NPs with two different diameters; d) a mixture of spherical Au and SiO$_2$ NPs. Insets show high-magnification images of the densely packed NP arrays. e) Optical images of CTAB-induced self-assembled 3D Pickering emulsions formed with Au NPs. Scale bars in (a)–(d) and in the insets of (a)–(d) correspond to 500 and 100 nm, respectively. The scale bar in (e) corresponds to 1 mm.

**ADVANCED
SCIENCE NEWS**

www.advancedsciencenews.com

**ADVANCED
MATERIALS
INTERFACES**

www.advmatinterfaces.de

to their irregular morphologies, while the monodispersed SiO₂ nanospheres were arranged into defect-free hexagonal arrays. Figure 5c,d shows SEM images of composite NP monolayers formed using a mixture of small (≈60 nm in diameter) and large (≈220 nm in diameter) Pt nanospheres and a mixture of SiO₂ and Au (both ≈50 nm in diameter) nanospheres, respectively. Surprisingly, even in areas where different types of particles were packed against each other, these composite arrays still self-arranged into densely packed hexagonal arrays like those formed using single types of monodispersed nanospheres (Figure 5c,d inset). From Figure 5c,d, it can also be seen that the differently sized Pt NPs mixed randomly with each other in the composite array while islands of different types of particles formed in the SiO₂-Au composite array. This dramatic contrast in mixing behavior is most likely due to the difference in surface chemistry of the NPs, which arises from the capping agents initially on the surface of the particles.[44] In the composite Pt array, although the Pt NPs are different in size, they all carry a layer of citrate on their surfaces. This gives the Pt NPs similar surface properties, which results in the differently sized Pt NPs packing randomly against each other. Conversely, in the SiO₂-Au composite array, the surfaces of SiO₂ and Au NPs are covered in layers of hydroxide and citrate, respectively, which gives the SiO₂ and Au NPs very different surface properties and leads them to pack as islands. It is notable that these important insights would not have been possible to obtain with conventional modifier methods for inducing self-assembly since they all result in significant changes to the surface chemistry of the NPs.

Finally, CTAB can also be readily used to promote the formation of 3D Pickering emulsions, which is demonstrated in Figure 5e with Au NPs. It is now well established that for NPs to effectively stabilize the curved liquid meniscus from coalescing in Pickering emulsions the surface of the NPs must exhibit appropriate hydrophobicity, which we have shown for Au NPs can be conveniently achieved by functionalizing the surface of the NPs with MPS ligands.[45] However, since MPS-functionalized NPs are negatively charged, this makes CTAB promoters, which can screen interparticle electrostatic repulsion without replacing MPS on the surface of the NPs, crucial for the formation of stable Au Pickering emulsions.

3. Conclusion

In summary, we have shown that CTAB, which is extensively used in colloidal synthesis and is therefore often inherently present in many colloidal NP suspensions, can act readily as a charge screening promoter to induce self-assembly of negatively charged colloidal NPs into densely packed multi-dimensional arrays at LLIs. Since this promoter mechanism is purely electrostatic and does not involve material-specific chemical adsorption, CTAB can be readily used as a general promoter for inducing self-assembly of negatively charged colloidal NPs regardless of their morphology, surface chemistry, or material composition. Since CTAB acts as a promoter to induce NP self-assembly, it does not replace the initial chemical species on the surface of the NPs and therefore avoids significant changes to the surface chemistry or local ionic balance of the colloidal particles. This is crucial for the formation of surface-active and defect-free NP

arrays, which is important for both fundamental research and real-life applications. Interestingly, it was also found that CTAB induced self-assembly of citrate-stabilized Au NPs through a concentration-dependent dual mechanism. At relatively high concentrations, CTAB induced self-assembly by acting as a charge-removing modifier while at lower concentrations CTAB predominately induced self-assembly by acting as a charge-screening promoter. This unique property of CTAB makes it the first chemical compound which has the ability to induce interfacial self-assembly as both a modifier and promoter and explains several recent observations in literature where citrate-stabilized Au nanorod colloids containing trace amounts of CTAB could spontaneously assemble into densely packed monolayers at LLIs.

4. Experimental Section

Materials: All chemicals used were ACS reagents purchased from Sigma Aldrich and were used without further purification. SiO₂ colloid (50 nm diameter, −46.8 mV zeta potential, 9.1 × 10¹³ particles mL⁻¹) was obtained from nanoComposix Inc. Aqueous P25 TiO₂ colloid (40 wt%) was obtained from Evonik. All experiments used low TOC (<3.0 ppb) 18.2 MΩ cm water.

Colloid Preparations: CRGC, citrate-reduced silver colloid, and citrate-reduced platinum colloid were synthesized following protocols reported in literature.[46–48] Commercial SiO₂ colloids were diluted by ×1000 before use. Commercial TiO₂ colloids were diluted by ×2000. The pH value of the diluted TiO₂ colloids was tuned to 11 using NaOH (aq.) so that they had a typical zeta potential of −30 mV.

Surface Modifications of CRGC: Surface modifications of CRGC with 3-mercapto-1-propane sulfonate sodium (MPS) and 2-mercapto-5-benzimidazolesulfonate sodium (MBS) were performed by pipetting 100 µL of 10⁻⁴ M thiol (aq.) solution into 5 mL CRGC followed by gentle stirring for 15 min. Thiocholine was synthesized following a method reported in literature.[49] Surface modifications of CRGC with thiocholine chloride (TC) were performed following a method previously reported.[50]

Interfacial NP Self-Assembly: To prepare 2D NP arrays with large area sizes for SEM, typically a mixture of 5 mL of aqueous NP colloid along with 3 mL of DCM and 80 µL of 10⁻⁵ M CTAB (aq.) was vigorously shaken for ≈30 s in a 50 mL polypropylene centrifuge tubes (Corning Incorporated). This resulted in the formation of particle-covered emulsions, which would coalesce to form an interfacial NP array. The particle density of the NP array would vary depending on the particle concentration of the parent colloid. Under the exact experimental parameters described above, the number of particles required to generate a densely packed 2D NP array was 5 × 10¹¹ particles mL⁻¹. NP arrays containing two different types of particles were fabricated by premixing the two particle colloids together (1:1 volume ratio) prior self-assembly. Au Pickering emulsions were fabricated by vigorously shaking 5 mL of aqueous colloid with 1 mL of DCM, 100 µL of 10⁻⁵ M MPS, and 80 µL of 10⁻⁵ M CTAB for 1 min.

Instrumentations: UV–vis spectra were recorded using an Agilent 8543 single beam diode array spectrophotometer. For SEM measurements, the interfacial NP arrays were anchored in situ onto a thin polystyrene backing to preserve their initial structures at the LLI using a method previously reported.[30] SEM was performed with a Quanta FEG 250 at an acceleration voltage of 30 kV under high chamber vacuum (under 8 × 10⁻⁵ mbar) with standard SEM copper tape. Samples containing SiO₂ or TiO₂ NPs were sputtered with Au (2 nm thick) prior to imaging. Zeta potentials of colloids were measured using a ZetaSizer Nano ZS. All samples were measured at 25 °C and on average three times in electrophoretic capillary cells. The cells were rinsed with absolute ethanol and then with water each time before use. SERS measurements of aggregated CRGC were acquired on the Avalon Raman Station which was equipped with a 100 mW 785 nm laser, using a total accumulation time of 20 s and 200 µL of as-prepared colloid mixed with 20 µL of 1 M

$(NH_4)_2SO_4$ (aq.) as the sample. CRGC MeLLF samples for SERS were prepared by shaking 0.9 mL of as-prepared aqueous colloid with 0.4 mL of DCM and 0.1 mL of CTAB (aq.). After MeLLF formation, 0.9 mL of the aqueous phase and 0.1 mL of DCM were removed from the sample before the sample was poured into 96 well-plates. These samples were analyzed using a Perkin Elmer RamanMicro 200F Microscope equipped with a 785 nm laser (60 μm diameter spotsize) with 20 s accumulation time and 40 mW laser power.

[1]   E. Roduner, *Chem. Soc. Rev.* **2006**, *35*, 583.
[2]   J. B. Edel, A. A. Kornyshev, M. Urbakh, *ACS Nano* **2013**, *7*, 9526.
[3]   L. Liu, A. Corma, *Chem. Rev.* **2018**, *118*, 4981.
[4]   Z. Nie, A. Petukhova, E. Kumacheva, *Nat. Nanotechnol.* **2010**, *5*, 15.
[5]   Y. Montelongo, D. Sikdar, Y. Ma, A. J. S. McIntosh, L. Velleman, A. R. Kucernak, B. J. Edel, A. A. Kornyshev, *Nat. Mater.* **2017**, *16*, 1127.
[6]   D. M. Scanlon, E. Smirnov, T. J. Stockmann, P. Peljo, *Chem. Rev.* **2018**, *118*, 3722.
[7]   H. K. Lee, Y. H. Lee, G. C. Phan-Quang, X. Han, C. S. L. Koh, X. Y. Ling, *Chem. Mater.* **2017**, *29*, 6563.
[8]   S. G. Booth, R. A. W. Dryfe, *J. Phys. Chem. C* **2015**, *119*, 23295.
[9]   Z. Niu, Y. Li, *Chem. Mater.* **2014**, *26*, 72.
[10] P. M. Konrad, A. P. Doherty, S. E. J. Bell, *Anal. Chem.* **2013**, *85*, 6783.
[11] R. McGorty, J. Fung, D. Kaz, V. N. Manoharan, *Mater. Today* **2010**, *13*, 34.
[12] H. Duan, D. Wang, D. G. Kurth, H. Möhwald, *Angew. Chem., Int. Ed.* **2004**, *43*, 5639.
[13] T. Ding, A. W. Rudrum, L. O. Herrmann, V. Turek, J. J. Baumberg, *Nanoscale* **2016**, *8*, 15864.
[14] F. Reincke, S. G. Hickey, W. K. Kegel, D. Vanmaekelbergh, *Angew. Chem., Int. Ed.* **2004**, *43*, 458.
[15] X. Lu, Y. Huang, B. Liu, L. Zhang, L. Song, J. Zhang, A. Zhang, T. Chen, *Chem. Mater.* **2018**, *30*, 1989.
[16] S. Si, W. Liang, Y. Sun, J. Huang, W. Ma, Z. Liang, Q. Bao, L. Jiang, *Adv. Funct. Mater.* **2016**, *26*, 8137.
[17] Y. Xu, M. P. Konrad, W. W. Y. Lee, Z. Ye, S. E. J. Bell, *Nano Lett.* **2016**, *16*, 5255.
[18] L. Velleman, D. Sikdar, V. A. Turek, A. R. Kucernak, S. J. Roser, A. A. Kornyshev, J. B. Edel, *Nanoscale* **2016**, *8*, 19229.
[19] S. Lin, X. Lin, Y. Shang, S. Han, W. Hasi, L. Wang, *J. Phys. Chem. C* **2019**, *123*, 24714.
[20] X. Lin, W.-L.-J. Hasi, S.-Q.-G.-W. Han, X.-T. Lou, D.-Y. Lin, Z.-W. Lu, *Phys. Chem. Chem. Phys.* **2015**, *17*, 31324.
[21] L. Tian, M. Su, F. Yu, Y. Xu, X. Li, L. Li, H. Liu, W. Tan, *Nat. Commun.* **2018**, *9*, 3642.
[22] K. Kim, H. S. Han, I. Choi, C. Lee, S. Hong, S.-H. Suh, L. P. Lee, T. Kang, *Nat. Commun.* **2013**, *4*, 2182.
[23] D. C. E. Calzolari, D. Pontoni, M. Deutsch, H. Reichert, J. Daillant, *Soft Matter* **2012**, *8*, 11478.
[24] L. Costa, G. Li-Destri, N. H. Thomson, O. Konovalov, D. Pontoni, *Nano Lett.* **2016**, *16*, 5463.
[25] F. Ravera, E. Santini, G. Loglio, M. Ferrari, L. Liggieri, *J. Phys. Chem. B* **2006**, *110*, 19543.
[26] M. Grzelczak, J. Pérez-Juste, P. Mulvaney, L. M. Liz-Marzán, *Chem. Soc. Rev.* **2008**, *37*, 1783.
[27] S. K. Mehta, S. Kumar, S. Chaudhary, K. K. Bhasin, M. Gradzielski, *Nanoscale Res. Lett.* **2009**, *4*, 17.
[28] X. Ye, C. Zheng, J. Chen, Y. Gao, C. B. Murray, *Nano Lett.* **2013**, *13*, 765.
[29] J. G. Mehtala, D. Y. Zemlyanov, J. P. Max, N. Kadasala, S. Zhou, A. Wei, *Langmuir* **2014**, *30*, 13727.
[30] Y. Xu, M. P. Konrad, J. L. Trotter, C. P. McCoy, S. E. J. Bell, *Small* **2017**, *13*, 1602163.
[31] M. Mabuchi, T. Takenaka, Y. Fujiyoshi, N. Uyeda, *Surf. Sci.* **1982**, *119*, 150.
[32] E. López-Tobar, B. Hernández, A. Chenal, Y.-M. Coïc, J. G. Santos, E. Mejía-Ospino, J. V. Garcia-Ramos, M. Ghomi, S. Sanchez-Cortes, *J. Raman Spectrosc.* **2017**, *48*, 30.
[33] Z. Ye, C. Li, Y. Xu, S. E. J. Bell, *Analyst* **2019**, *144*, 448.
[34] A. L. Dendramis, E. W. Schwinn, R. P. Sperline, *Surf. Sci.* **1983**, *134*, 675.
[35] Y. Liang, N. Hilal, P. Langston, V. Starov, *Adv. Colloid Interface Sci.* **2007**, *134–135*, 151.
[36] J. A. da Silva, M. R. Meneghetti, *Langmuir* **2018**, *34*, 366.
[37] Y. Gao, L. Li, X. Zhang, X. Wang, W. Ji, J. Zhao, Y. Ozaki, *Chem. Commun.* **2019**, *55*, 2146.
[38] R. Tadmouuri, C. Zedde, C. Routaboul, J.-C. Micheau, V. Pimienta, *J. Phys. Chem. B* **2008**, *112*, 12318.
[39] V. Pimienta, M. Brost, N. Kovalchuk, S. Bresch, O. Steinbock, *Angew. Chem., Int. Ed.* **2011**, *50*, 10728.
[40] P. Peljo, E. Vladimirova, E. Smirnov, G. Gschwend, L. Rivier, H. H. Girault, *J. Phys. Chem. C* **2018**, *122*, 18510.
[41] M. Anyfantakis, J. Vialetto, A. Best, G. K. Auernhammer, H.-J. Butt, B. P. Binks, D. Baigl, *Langmuir* **2018**, *34*, 15526.
[42] F. Reincke, K. W. Kegel, H. Zhang, M. Nolte, D. Wang, D. Vanmaekelbergh, H. Möhwald, *Phys. Chem. Chem. Phys.* **2006**, *8*, 3828.
[43] M. L. Donten, A. Królikowska, J. Bukowska, *Phys. Chem. Chem. Phys.* **2009**, *11*, 3390.
[44] A. Sánchez-Iglesias, M. Grzelczak, J. Pérez-Juste, L. M. Liz-Marzán, *Angew. Chem., Int. Ed.* **2010**, *49*, 9985.
[45] Z. Ye, C. Li, N. Skillen, Y. Xu, H. McCabe, J. Kelly, P. Robertson, S. E. J. Bell, *Appl. Mater. Today* **2019**, *15*, 398.
[46] N. G. Bastús, J. Comenge, V. Puntes, *Langmuir* **2011**, *27*, 11098.
[47] P. C. Lee, D. Meisel, *J. Phys. Chem.* **1982**, *86*, 3391.
[48] K. Kim, K. L. Kim, H. B. Lee, K. S. Shin, *J. Phys. Chem. C* **2010**, *114*, 18679.
[49] B. J. Walker, A. Dorn, V. Bulović, M. G. Bawendi, *Nano Lett.* **2011**, *11*, 2655.
[50] A. Stewart, S. Murray, S. E. J. Bell, *Analyst* **2015**, *140*, 2988.